

## Review of minimum-bias jet systematics at RHIC

---

**Duncan Prindle\*** for the STAR Collaboration

*University of Washington*

*E-mail:* [prindle@npl.washington.edu](mailto:prindle@npl.washington.edu)

Jets are studied in A-A collisions at RHIC and LHC with the goal to understand how they are affected by the medium and how they affect the medium. It is widely believed that hard-scattered partons lose energy when propagating through a medium before hadronizing. Partons losing enough energy may not even make it out of the medium as identifiable jets (although the momentum will be shared among whatever particles are emitted). “Full” jet reconstruction attempts to determine the partonic energy loss as well as possible changes in jet shape. Heavy ion collisions typically produce many unrelated particles within the jet “cone,” and subtraction of this background introduces significant uncertainties. A variety of techniques using high- $p_t$  particles, assumed to be leading particles from jet fragmentation, look for disappearance of jets and attenuation of jets relative to the reaction plane, as well as medium modifications such as Mach cones. Those techniques have considerable uncertainty due to subtraction of  $v_2$ . In this paper we discuss minimum-bias jets observed at RHIC using two-particle correlations. We find that jets produced in p-p collisions have interesting properties. Peripheral A-A collisions look like p-p collision. As we select more central collisions the number of jets increases following binary collision scaling until at a system-dependent centrality the number of particles associated with jets increases substantially above this scaling. Near this transition centrality the jet aspect ratio—elongated transverse to the beam direction for low-energy jets produced in p-p collisions—becomes highly elongated along the beam direction in A-A collisions.

*Workshop on Critical Examination of RHIC Paradigms*

*April 14, 2010*

*Austin, Texas, U.S.A.*

---

\*Speaker.

## 1. Introduction

Our studies of two-particle correlations began in the late 1990's with the desire to understand heavy-ion collisions in an unbiased way [1]. At that time it was expected that central A-A collisions would be nearly thermalized with jets quenched and, if not completely absorbed, difficult to observe. Temperatures inferred from  $p_t$  spectra could fluctuate event to event or from place to place within an event, the amplitude and volume of  $p_t$  fluctuations depending on the nearness of the event to the quark-gluon plasma phase boundary. We wanted to observe these fluctuations in an unambiguous way.

A number of techniques were considered, such as factorial moments [2] [3], wavelets [4] and entropy transport [5]. But those measurements are logarithmic in the scale, and we soon realized that the range of scales available to a detector like STAR was at best two orders of magnitude, making a measure linear in scale preferable. We eventually settled on measures related to variance differences and learned how to convert between correlations and fluctuations. [6] These correlation measures can be related to Pearson's correlation coefficient, making them more easily interpretable than fluctuations which are integrals over correlations and thus include correlation structure from many scales.

There were some concerns about whether such a general approach could work, partly fueled by previous difficulty interpreting factorial moments [7] [8]. Also, it is easy for a detector artifact to produce a signal which may confuse the physics interpretation. With a variance-based measure it is possible to cancel detector artifacts in a natural way using mixed events. It was also believed that a generic two-particle correlation analysis wouldn't be sensitive enough to see correlations such as flow. Monte Carlo simulations of temperature fluctuations within nearly-thermalized events were performed and it was shown that our techniques could measure the fluctuations that were expected at that time. In fact we could distinguish the case where events were thermalized with each event having a different temperature from the case where events were nearly thermalized but having a temperature that varied with position [9]. When we analyzed collision data we saw considerable correlation structure, but no evidence for temperature fluctuations [10].

There are several structures apparent in two-particle correlations. These are typically different enough in angular size that we can disentangle them. There is a very sharp  $e^+e^-$  peak due to  $\gamma$ -induced pair production. The observed HBT peak is broader than the  $e^+e^-$  peak but narrower than the same-side (SS) 2D peak due to minijets. When they are similar sizes we can use the fact that HBT is only observed for like-sign (LS) pairs while minijets have a strong unlike-sign (US) component. Back-to-back scattered partons are observed as an away-side (AS) ridge (as well as both partons contributing to the SS 2D peak) and this ridge is approximately independent of  $\eta_\Delta = \eta_1 - \eta_2$  within the STAR TPC acceptance. For high  $p_t$  particles we expect the AS ridge to be a Gaussian centered at  $\pi$  on  $\phi_\Delta = \phi_1 - \phi_2$ , but when that Gaussian is broad enough in  $\phi_\Delta$  (as it is for most of our  $p_t$  range) it has a  $\cos(\phi_\Delta - \pi)$  shape. We refer to  $\cos(\phi_\Delta - \pi)$  as an azimuth dipole. There is also a quadrupole observed,  $\cos(2\phi_\Delta)$ . The dipole and quadrupole are orthogonal to each other on  $\phi_\Delta$  and distinguished from HBT and the SS 2D Gaussian minijet peak by their long ranges in  $\eta_\Delta$ .

In the rest of this paper we emphasize the jet-like components of two-particle correlations. We start with a discussion of two-particle correlation measurement techniques, noting the equivalence

of fluctuations and correlations, and discuss how to interpret the multi-dimensional two-particle correlation space. Then we examine p-p collisions, the reference system for A-A collisions, and find interesting two-particle correlation structure. We next see how some of this structure is modified in A-A collisions. Finally we make some comments about how  $p_t$  correlations complement number correlations.

## 2. Review of Methods

Jets can be defined by a jet-finding algorithm which groups all particles that come from the fragmentation of a hard-scattered parton [11][12][13]. There are a few commonly used algorithms. It is an active area of research to determine which ones work best in a heavy ion collision environment. How well these algorithms work depends on the jet shape, which could depend on a jet-medium interaction as well as the fluctuating background of hadrons unrelated to the particular scattered parton. An alternative to explicit jet reconstruction is to study two-particle correlations. This approach makes no assumption about jet shapes and allows one to study lower-energy partons than explicit jet reconstruction algorithms permit. Indeed, below a few GeV, partons will only be able to fragment into two hadrons, and this is difficult to observe with jet reconstruction algorithms in heavy ion environments. Another advantage of two-particle correlations is that they allow study of inter-jet correlations as well as intra-jet correlations.

The most common measure of the dependence between two statistical quantities is Pearson's correlation coefficient [14], the covariance divided by the geometric mean of variances, which is bounded by -1 and 1. We are interested in the structure of two-particle momentum-space correlations. We write the covariance  $\Delta\rho$  as a difference between an object and a reference,

$$\begin{aligned}\Delta\rho(\vec{p}_1, \vec{p}_2) &= \rho_{sib}(\vec{p}_1, \vec{p}_2) - \rho_{ref}(\vec{p}_1, \vec{p}_2) \\ &= \rho_{(2)}(\vec{p}_1, \vec{p}_2) - \rho_{(1)}(\vec{p}_1)\rho_{(1)}(\vec{p}_2)\end{aligned}$$

where  $\rho_{(2)}$  is a two-particle density and  $\rho_{(1)}$  is a one-particle density. In practice we bin quantities, storing them in histograms. For the case of number correlations the bin  $(a, b)$ , representing correlations between particles at positions a and b, can be written as

$$\varepsilon_a \varepsilon_b \Delta\rho(n) = \langle n_a n_b \rangle - \langle n_a \rangle \langle n_b \rangle = \overline{(n - \bar{n})_a (n - \bar{n})_b}$$

where  $\varepsilon$  are the bin widths. For Pearson's correlation coefficient we divide by the geometric mean of the variances,  $\Delta\rho / \sqrt{\sigma_{n_a}^2 \sigma_{n_b}^2} \approx \Delta\rho / \sqrt{\bar{n}_a \bar{n}_b} = \Delta\rho / \sqrt{\rho_{ref}}$ . We have replaced the variances in the denominator with the Poisson expectations so that all the physics is in the numerator. In a detector one must deal with efficiencies and acceptances. The quantity we actually use is thus

$$\sqrt{\rho'_{ref}} \frac{\Delta\rho}{\rho_{ref}}.$$

We normally refer to this simply as  $\Delta\rho / \sqrt{\rho_{ref}}$ . We define  $\sqrt{\rho'_{ref}} \equiv \frac{d^2 N}{d\eta d\phi}$ . The ratio  $\Delta\rho / \rho_{ref}$  has the virtue of canceling efficiencies and acceptances. Besides being closely related to a standard correlation measure the quantity  $\Delta\rho / \sqrt{\rho_{ref}}$  is the correlation strength per final-state particle. If

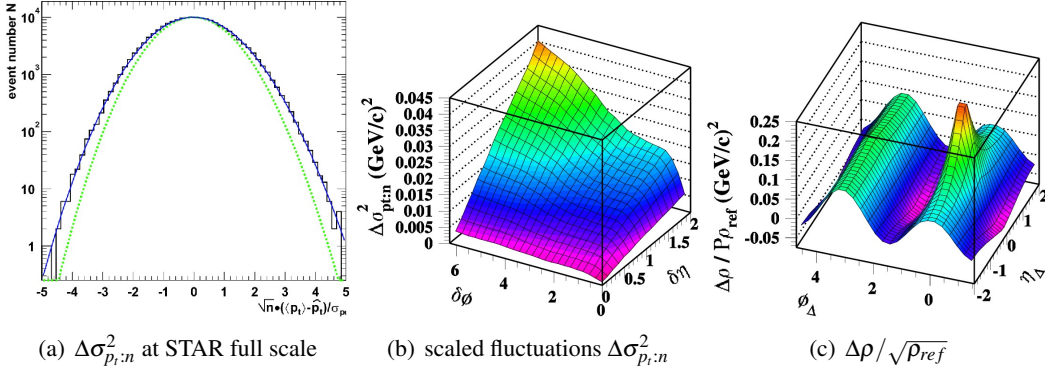


**Figure 1:** Sequence going from measurement of fluctuations at STAR full scale to scaled fluctuations probing dependence on size and finally to correlations inferred from fluctuations. There is an interesting structure in the correlations.

A-A collisions are simply superpositions of N-N collisions it will be independent of centrality and collision system.

Correlations and fluctuations are closely related, fluctuations resulting from an integral over the correlation structure. For the angular space the integral equation relating the fluctuations and correlations is [6]

$$\Delta\sigma_{p_t;n}^2(\delta\eta, \delta\phi) = 4 \int_0^{\delta\eta} d\eta_\Delta \int_0^{\delta\phi} d\phi_\Delta K(\delta\eta, \delta\phi; \eta_\Delta, \phi_\Delta) \frac{\Delta\rho}{\sqrt{\rho_{ref}}}(\eta_\Delta, \phi_\Delta),$$

where  $\Delta\sigma_{p_t;n}^2(\delta\eta, \delta\phi)$  is a variance difference measured in a “detector” of size  $(\delta\eta, \delta\phi)$ , the kernel  $K$  is an exactly known geometric factor and  $\Delta\rho/\sqrt{\rho_{ref}}$  is a two-particle autocorrelation. This form of integral equation is known as a Volterra equation. Writing this equation in terms of binned quantities we can evaluate the kernel explicitly (Eq. 5 of [16])

$$\Delta\sigma_{p_t;n}^2(\delta\eta, \delta\phi) = 4 \sum_{k=1}^{k=m} \sum_{l=1}^{l=n} \left(1 - \frac{k-1/2}{m}\right) \left(1 - \frac{l-1/2}{n}\right) \frac{\Delta A}{\sqrt{A_{ref}}}(k\varepsilon_\eta, l\varepsilon_\phi).$$

Here we use  $A$  instead of  $\rho$  to indicate it is a binned quantity. We see that in general fluctuations depend on the domain scale over which they are measured. When we measure fluctuations at a particular scale we have an integral of the correlations up to that scale. The difference in fluctuations between two scales is a measure of the integral of the correlations between those scales. We can measure the scale dependence of  $\Delta\sigma_{p_t;n}^2$  on  $(\delta\eta, \delta\phi)$  and invert the integral equation to infer  $\frac{\Delta\rho}{\sqrt{\rho_{ref}}}(\eta_\Delta, \phi_\Delta)$ . Inverting Volterra equations (to solve for correlations from fluctuations) is an example of an ill-posed problem. One must impose a regularization scheme to obtain a useful solution, analogous to applying a low-pass filter. There is a well-developed mathematical framework for this [15] but one always has to assess how much the regularization scheme affects the extracted correlations. An example of inverting scaled fluctuations to get correlations is shown in Fig. 1 [17][18]. We note that one motivation for measuring mean- $p_t$  fluctuations was to determine event-to-event temperature fluctuations. The correlation structure we observe is inconsistent with temperature fluctuations, instead it reveals jet correlations.

Fluctuations are less numerically expensive to compute than correlations but they are difficult to interpret. We can invert the integral equation to get the more-easily interpretable correlation

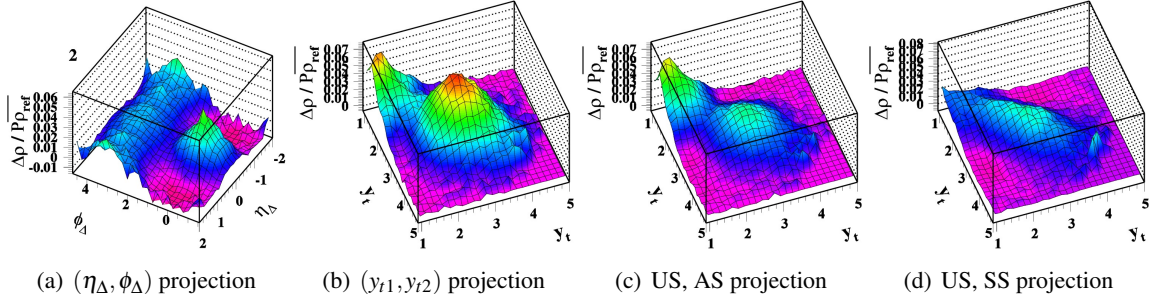


**Figure 2:** Projections of the six dimensional correlation space onto two dimensional subspaces for p-p collisions. Panel 2(a) is the projection onto the angular subspace,  $(\eta_\Delta, \phi_\Delta)$ , with a “hard”  $p_t$  cut imposed. We see an intra-jet correlation on the same-side (SS) and an inter-jet ridge on the away-side (AS); the ridge is due to the fact that the parton center of mass is not at rest in the laboratory frame. Panel 2(b) is the full space projected onto the  $(y_{t1}, y_{t2})$  subspace. Panels 2(c) and 2(d) are projections of the AS and SS correlations of unlike-sign (US) pairs onto the  $(y_{t1}, y_{t2})$  subspace.

structure, but the issue with regularization will always be a source of uncertainty. There are also technical issues such as two-track resolution that are difficult to correct in a fluctuation measure. Having established a direct connection [6] we prefer to measure angular correlations directly.

Each particle has three momentum components, so the two-particle correlation space is six dimensional. In a detector with complete azimuthal coverage the absolute position of the pair ( $\phi_\Sigma = \phi_1 + \phi_2$ ) does not matter. Only the difference  $\phi_\Delta$  matters. Within the  $\eta$  acceptance of the STAR TPC it is approximately true that pair correlations are independent of  $\eta_\Sigma \equiv \eta_1 + \eta_2$ , depending only on difference  $\eta_\Delta$ . Averaging over  $\phi_\Sigma$  and  $\eta_\Sigma$  reduces the dimensionality of the correlation space to four with no loss of information.

We are still left with a four-dimensional space, two angle differences and two momentum magnitudes. It is common to use  $p_t$  for the momentum magnitude, but since the yield falls steeply with  $p_t$  most of the pairs occupy a small corner of the relevant  $(p_{t1}, p_{t2})$  space. We use  $y_t \equiv \ln[(m_t + p_t)/m_\pi]$  for better visual access to the low- $p_t$  correlation structure. Four dimensions is impossible to visualize so we project onto the 2D angular subspace,  $(\eta_\Delta, \phi_\Delta)$ , which has the form of a joint autocorrelation, or the 2D  $(y_{t1}, y_{t2})$  subspace. It is instructive to make cuts on the space that is projected out. In Fig. 2 we show examples of projections onto the  $(\eta_\Delta, \phi_\Delta)$  and  $(y_{t1}, y_{t2})$  subspaces. For the  $(y_{t1}, y_{t2})$  subspace we show the projection over the full angular space as well as for the AS and the SS.

### 3. Two-particle correlations from proton-proton collisions

In this section we examine the two-particle correlation structure of particles produced in p-p collisions. First we make a connection with a spectrum analysis in which events with different numbers of observed charged particles ( $n_{ch}$ ) were analyzed separately. It was observed that one can define a “soft” component. When the soft component is subtracted from each of the  $n_{ch}$  spectra what remains has a shape and position independent of  $n_{ch}$ , but an amplitude proportional to  $n_{ch}$ —the so-called “hard” component [19]. When plotted on  $y_t$  the hard-component shape is Gaussian with a peak at  $y_t = 2.7$  or  $p_t = 1$  GeV/c. This is the same position of the peak we find in the

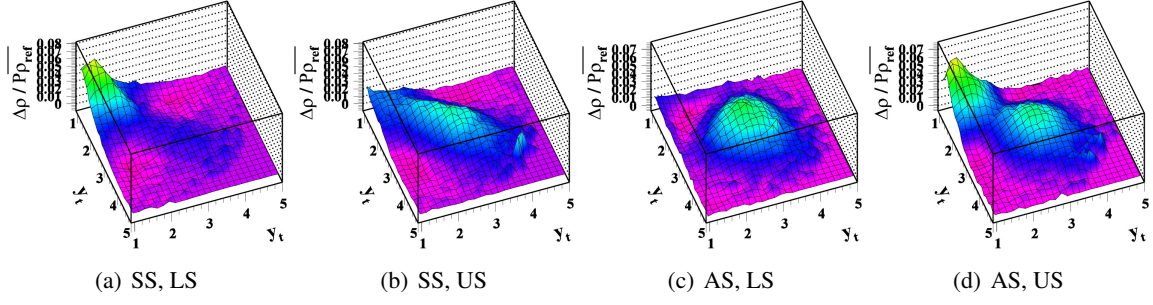


**Figure 3:** Projections of two-particle correlations onto  $(y_{t1}, y_{t2})$  with cuts on angular space. The AS parton fragmentation region is independent of charge sign, the US pairs have additional soft component. The SS parton fragmentation region is restricted to US pairs.

projection of the two-particle correlations onto  $(y_{t1}, y_{t2})$  as shown in Fig. 2(b). In Fig. 5 we will see that for low- $y_{t\Sigma} \equiv y_{t1} + y_{t2}$  pairs the angular correlations are dominated by soft physics while for high- $y_{t\Sigma}$  pairs the angular correlations are dominated by hard scattering.

We examine  $(y_{t1}, y_{t2})$  in more detail by cutting on SS and AS pairs as well as looking at LS and US pairs. These four combinations are shown in Fig. 3. We refer to the region around  $y_t \approx 3$  ( $p_t \approx 1.5$  GeV/c) as the fragmentation region. We see that for the AS this region is independent of the charge combination. For SS pairs the fragmentation region is restricted to US pairs. These correlations are dominated by low- $Q^2 \approx 3$  GeV partons which primarily fragment into hadron pairs, the pair being charge neutral.

We have already seen in Fig. 2(a) that when projecting from the fragmentation region of  $(y_{t1}, y_{t2})$  the angular correlations have clear hard scattering (jet) structure. We can also ask how the shape of the  $(y_{t1}, y_{t2})$  correlations should look if it is really due to fragmentation. One can parameterize parton fragmentation functions (FFs) in a universal form [21]. This allows us to construct a 2D plot with the parton momentum along one axis and the fragment momenta along the other axis as shown in Fig. 4(a). A slice parallel to the fragment momentum axis is a fragmentation function. The amplitude of these slices is determined by the underlying parton spectrum. For large parton momentum the mode of the fragmentation function is well determined by pQCD [20][21]. As the parton energy decreases the number of hadrons it fragments to decreases until for some energy ( $\approx 3$  GeV) there are only two fragments (a parton may turn into a single hadron “fragment”, but we are studying two-particle correlations). We do not observe the parton, only the hadrons. So we symmetrize the parton versus fragment plot to get a fragment versus fragment plot, integrating over parton momentum as shown in Fig. 4(b). At low  $y_{t\Sigma}$  the yield is dominated by partons fragmenting to two hadrons and is peaked along the diagonal. As the fragment  $y_t$  increases the importance of parton fragmentation to three, four and more particles increases. The maximum in the  $(y_{t1}, y_{t2})$  plot deviates from the diagonal and follows the line of modes predicted by pQCD. This expectation is sketched in Fig. 4(b). Compare this to the measured  $(y_{t1}, y_{t2})$  correlation for SS fragments in Fig. 4(c).

We can also go in the other direction, from the data to the line of modes. We take the  $(y_{t1}, y_{t2})$  plot and project the conditional slices shown in Fig. 4(c) onto  $y_t$ . For relatively large  $y_t$  these are well described by a Gaussian with the same width determined from the spectrum analysis [19].

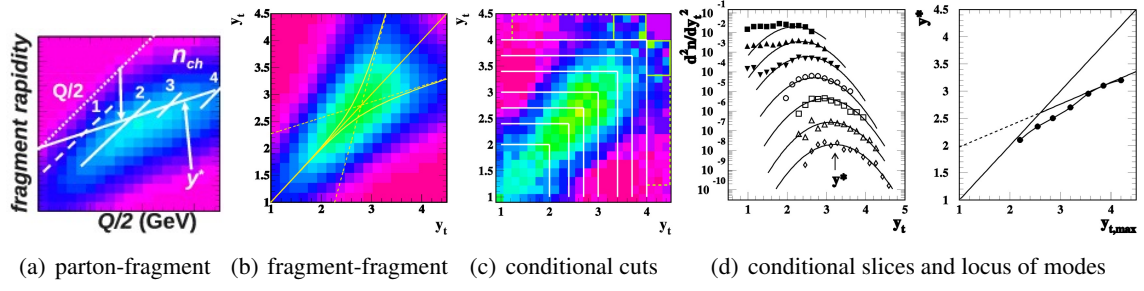


**Figure 4:** Panel 4(a) shows the parton momentum versus fragment momentum. A vertical slice projected onto fragment momentum is a fragmentation function. In panel 4(b) we symmetrize, integrating over parton momenta to get a figure we can compare to measurement. We note that at low momentum the fragment yield is dominated by partons fragmenting to two hadrons and is peaked along the diagonal. For larger momentum we can have parton to three or more fragments and we see the mode following the pQCD expectation. Panel 4(c) is the measured SS ( $y_{t1}, y_{t2}$ ) correlation which should be compared with 4(b). In panel 4(d) we show conditional slices for the cuts defined in panel 4(c), fitting them to get the modes of the fragmentation functions. These closely follow the expectation sketched in panel 4(b).

Using this width to fit all  $y_t$  slices works well down to  $y_t$  of about 2.5 ( $p_t \approx 1$  GeV/c). A plot of the Gaussian centroid versus  $y_t$  slice starts off along the diagonal then curves, following the expected pQCD line of modes. This is shown in Fig. 4(d) which should be compared with Fig. 4(b). The interpretation that the area around  $y_t \approx 3$  is due to fragmentation is supported not only by the shape of the angular correlations but also by details of measured fragmentation functions.

We now turn to the angular correlation dependence on the ( $y_{t1}, y_{t2}$ ) space. In Fig. 5 we show the angular correlations for LS and US pairs for “soft” ( $y_{t\Sigma} < 2.7$ ) and “hard” ( $y_{t1}, y_{t2} > 2$ ) pairs. We see a pronounced HBT signal in the LS pairs at (0,0), especially for the soft cut. The largest component of the soft US pairs is a 1D Gaussian on  $\eta_\Delta$  due to charge ordering in projectile nucleon fragmentation along the beam axis. Imposed on this is a dip centered at (0,0) due to momentum conservation (when there are only a few particles in an event they will be biased against having the same direction, unless they are fragments from a single hard-scattered parton) and a narrow peak at (0,0) due to  $e^+e^-$  from  $\gamma$ -induced pair production. The hard pairs have an AS ridge that is independent of charge, the SS peak is primarily in US pairs.

In Fig. 6 we examine this jet structure in more detail by making finer cuts on  $y_{t\Sigma}$ . As  $y_{t\Sigma}$  is increased the SS becomes sharper and the AS ridge becomes narrower. The width of the AS ridge is affected by  $k_t$ , a measure of the initial-state parton transverse momenta. The widths of the SS 2D Gaussian are related to  $j_{t\eta}$  and  $j_{t\phi}$ , measures of the transverse momentum with respect to the thrust axis of the fragmentation process [22][23]. The relations between the widths and the  $j_t$ s and  $k_t$  is usually derived for the asymmetric case of a leading particle [24][25]. In this analysis we use a formulation symmetric in the two particles [26]. In addition, since the most-probable parton has  $Q \approx 3$  GeV and the observed  $k_t$  is typically around 1 GeV/c (with the  $j_t$ s being not too much smaller) we cannot use small-angle approximations. When  $y_{t\Sigma}$  is comparable to  $j_t$  or  $k_t$  the fragment distributions will be affected by kinematic limits. The results of fits to the SS peak are shown in Fig. 6. Panel 6(a) shows the widths in the  $\eta_\Delta$  and  $\phi_\Delta$  directions. Since  $y_t$  is the log of  $p_t$  the x-axis is essentially  $1/p_t$ , the  $p_t$  of the pair decreasing from left to right. We see that for this

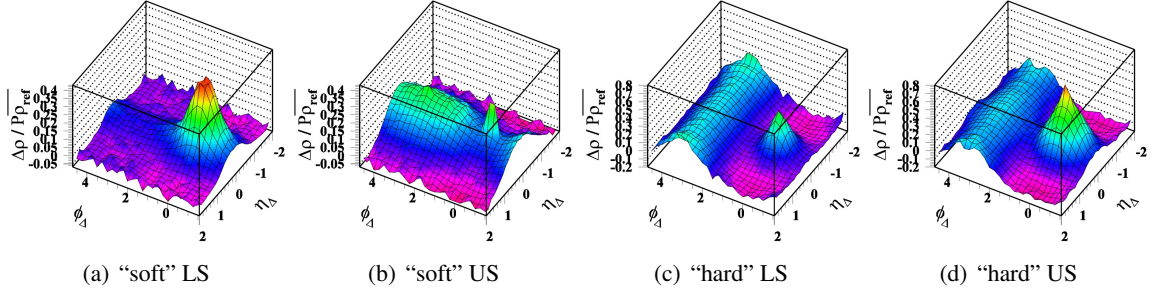


**Figure 5:** Projections of two-particle correlations onto  $(\eta_\Delta, \phi_\Delta)$  space with cuts on  $(y_{t1}, y_{t2})$  space. Soft pairs have  $y_{t1} + y_{t2} < 2.7$  and hard pairs  $y_{t1}, y_{t2} > 2$ . For the soft pairs the LS has a strong HBT component while the US is dominated by local measure conservation such as momentum and charge. For the hard pairs the AS ridge is charge independent while the SS jet peak is primarily US.

variable the  $\eta$  and  $\phi$  widths of the SS peak are approximately linear, but different from each other and dependent on charge combination. Panel 6(c) shows the inferred  $j_t$ s, this time plotted on  $y_{t\Sigma}$ . The difference in the  $j_{t\eta}$  and  $j_{t\phi}$  is greatest at low  $y_{t\Sigma}$ . As  $y_{t\Sigma}$  is increased they both increase until at large enough momentum they approach the observed perturbative  $j_t$ -scaling value [23].

The width of the AS ridge can be used to infer  $k_t$ , which has components from intrinsic initial-state parton momenta and initial-state radiation [27]. The momentum transfer between the scattered partons defines a direction  $\vec{q}$ . When the initial  $k_t$  of both partons is perpendicular to  $\vec{q}$  but parallel to each other the AS ridge width is widest. The effects of  $k_t$  also show up in the AS  $(y_{t1}, y_{t2})$  correlations. When the  $k_t$ s of the two partons are parallel to each other and parallel to  $\vec{q}$  the  $y_t$  values for the fragments of one of the partons will be boosted while the  $y_t$  for fragments of the other parton are reduced. This populates the off-diagonal region of the  $(y_{t1}, y_{t2})$  correlation. We show the AS  $(y_{t1}, y_{t2})$  correlation in panel 7(a). In contrast, the SS correlation, shown in panel 7(b), is unaffected by  $k_t$  and is considerably narrower. Typically, measured  $k_t$  is about 1 GeV/c, nearly the same momentum as the minijet partons we are probing. It may be possible in some cases for the  $k_t$  to boost the scattered partons enough so that they both actually emerge on the same side.

We have seen how we can use standard correlation measures to extract information in p-p collisions. We find clear signatures of hard parton scattering at surprisingly low parton momenta. We have also seen that there is a nice correspondence between two-particle correlations and a spectrum analysis which indicates a hard component appearing in perhaps 1% of NSD p-p collisions at 200 GeV [19]. We want to use this information as the baseline when analyzing A-A collisions, keeping in mind that the fraction of particles produced by hard scattering depends on centrality. So the superposition of N-N collisions should be weighted appropriately to account for the hard p-p spectrum component.

#### 4. Two-particle correlations in A-A collisions

In this paper we only discuss angular correlations from symmetric A-A collisions. We have analyzed Au-Au collisions at 200 GeV and 62 GeV as well as Cu-Cu collisions at the same energies. We see evolution with centrality from a correlation structure consistent with p-p collisions for the more peripheral events to a structure dominated by the SS 2D peak being strongly elongated



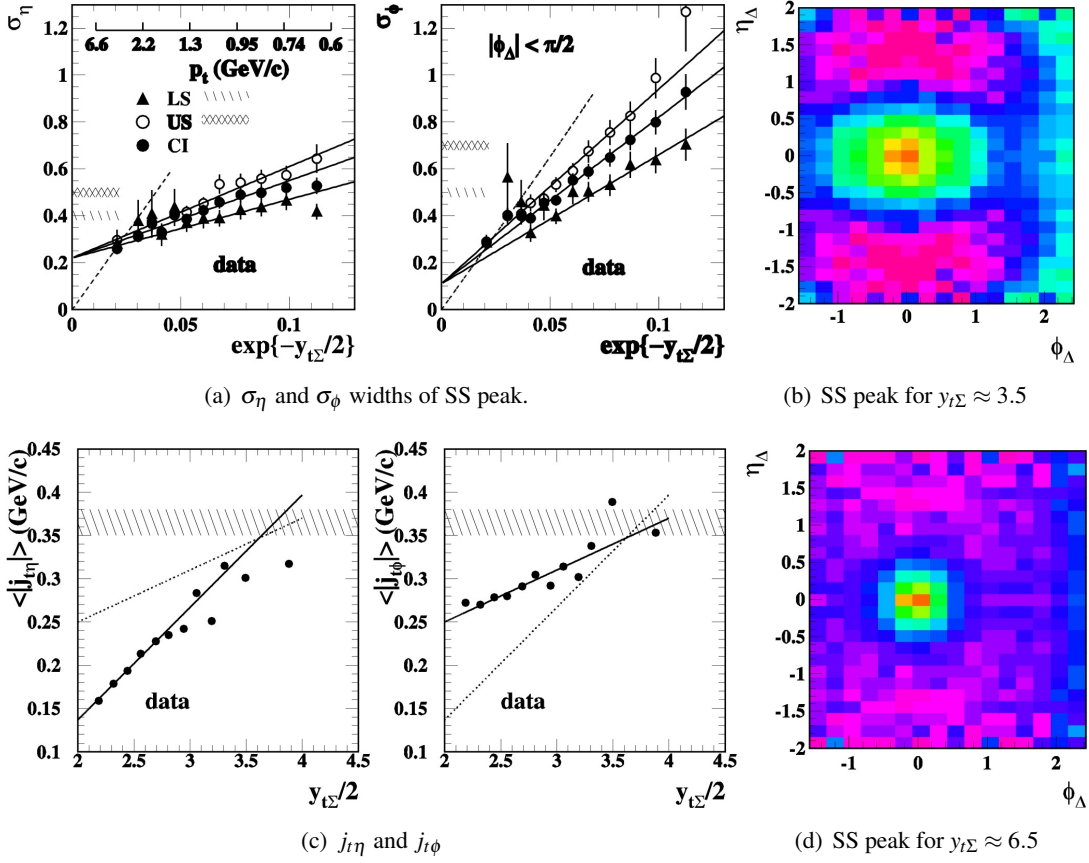


**Figure 6:** Panel 6(a) shows the fitted widths of the SS peak, the x-axis being essentially  $1/p_t$  of the pair. The widths depend on the direction ( $\eta$  or  $\phi$ ) and the charge combination but are approximately linear in this variable. Panel 6(c) shows the extracted  $j_t$  values for the  $\eta$  and  $\phi$  directions, having very different values for low  $y_t$  but approaching the  $j_t$  scaling value at high  $y_t$ . Panels 6(b) and 6(d) are projections onto  $(\eta_\Delta, \phi_\Delta)$  for low and high  $y_{t\Sigma}$  cuts and plotted in 1:1 aspect ratio and graphically showing the change in the shape of the SS peak as a function of pair momentum.

along  $\eta_\Delta$  and an AS ridge consistent with back-to-back hard parton scattering. For mid-central collisions there is in addition a  $\cos(2\phi_\Delta)$  quadrupole component. Examples for a few centralities of 200 GeV Au-Au collisions are shown in Fig. 8. The other collision systems are qualitatively similar.

We quantitatively describe the 2D correlation structure with a SS 2D Gaussian (with different  $\eta_\Delta$  and  $\phi_\Delta$  widths), a  $\cos(\phi_\Delta - \pi)$  dipole describing the AS ridge and a 1D Gaussian on  $\eta_\Delta$  [28]. To complete the description of p-p collisions we include a narrow exponential at the origin to describe  $e^+e^-$  pairs from  $\gamma$  conversions as well as an overall offset. We don't infer any physics from the exponential peak or the offset. This model function with ten parameters works well for the most peripheral and fairly well for the most central data. For intermediate centralities a  $\cos(2\phi_\Delta)$  term is required as well.

Fit parameters are shown in Fig. 9. The most striking feature of the fit parameters is that the SS Gaussian amplitude closely follows the expectation for binary scaling up to some centrality then greatly exceeds it. The AS ridge described by  $\cos(\phi_\Delta - \pi)$  tracks the amplitude of the SS Gaussian.

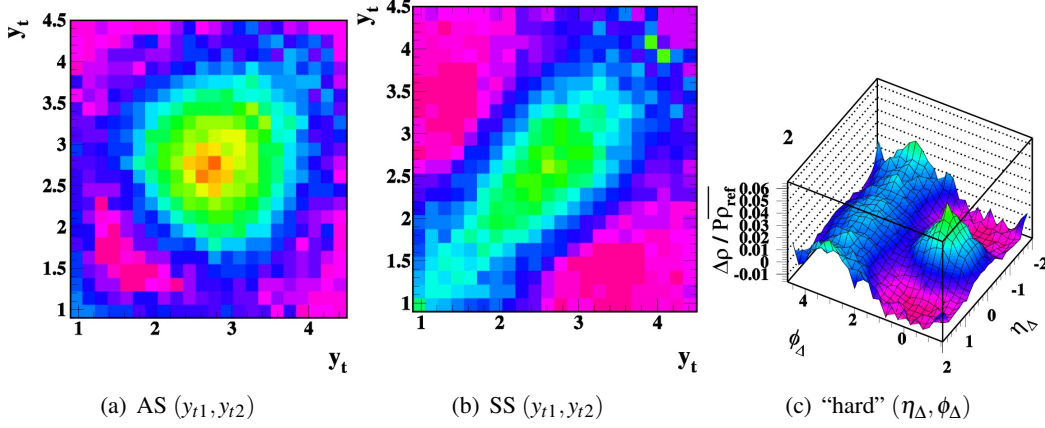


**Figure 7:** Effect of  $k_t$  on  $(y_{t1}, y_{t2})$  correlations. Panel 7(a) shows the AS ( $y_{t1}, y_{t2}$ ), broadened when the  $k_t$  of the two scattered partons are parallel to each other and the direction of the momentum transfer. The SS correlation, shown in panel 7(b), is not affected by  $k_t$ . Panel 7(c) indicates how one can extract  $k_t$  by measuring the width of the AS ridge.

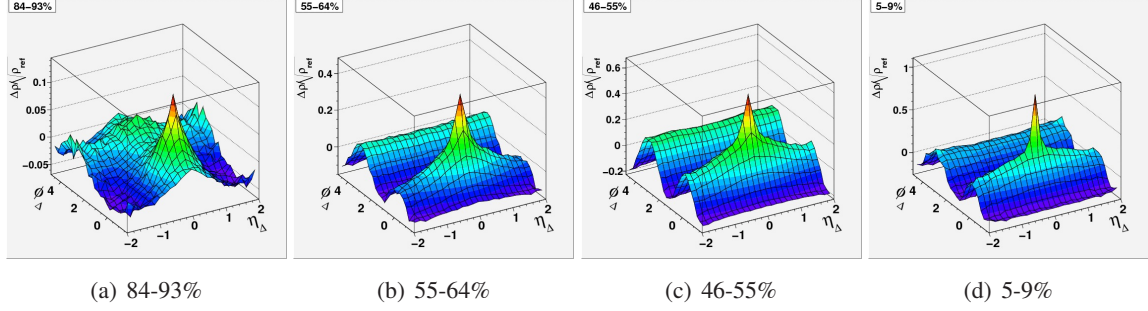


**Figure 8:** Samples of  $(\eta_\Delta, \phi_\Delta)$  correlations for 200 GeV Au-Au collisions. Panel 8(a) is most peripheral (84-94%) while panel 8(b) is nearly central. The middle two panels are on either side of the sharp transition, 55-64% and 46-55% centralities.

The  $\eta_\Delta$  width of the SS peak also increases greatly close to the same centrality. In contrast to the  $\eta_\Delta$  width, the  $\phi_\Delta$  width starts at the same value as we find for p-p collisions but then actually decreases. In contrast to the sharp transition of the jet amplitude the  $\cos(2\phi_\Delta)$  component has an *interesting but unrelated* evolution on centrality.

We emphasize the deformation of the SS Gaussian peak by plotting the data after subtracting the multipoles determined by the fit (we also subtract the sharp exponential peak) in Fig. 10, plotting the data in a one-to-one aspect ratio. The most peripheral bin is actually elongated along the  $\phi_\Delta$  direction. But as we increase centrality the peak becomes symmetric, then within a narrow centrality range becomes greatly elongated along  $\eta_\Delta$ .

In Fig. 11 we present an isometric view of the same data. We subtract the fitted dipole, quadrupole and sharp exponential peak from the data. The sharp peak affects only a few bins around the origin. Our parameterization of the data does a good job describing the  $\phi_\Delta$  structure of the AS peak. There is a small but statistically significant  $\eta_\Delta$  structure remaining on the AS. We note that the  $\phi_\Delta$  dependence of the SS 2D peak plotted here can be decomposed into Fourier components on azimuth and would contribute significantly to an inferred quadrupole component.

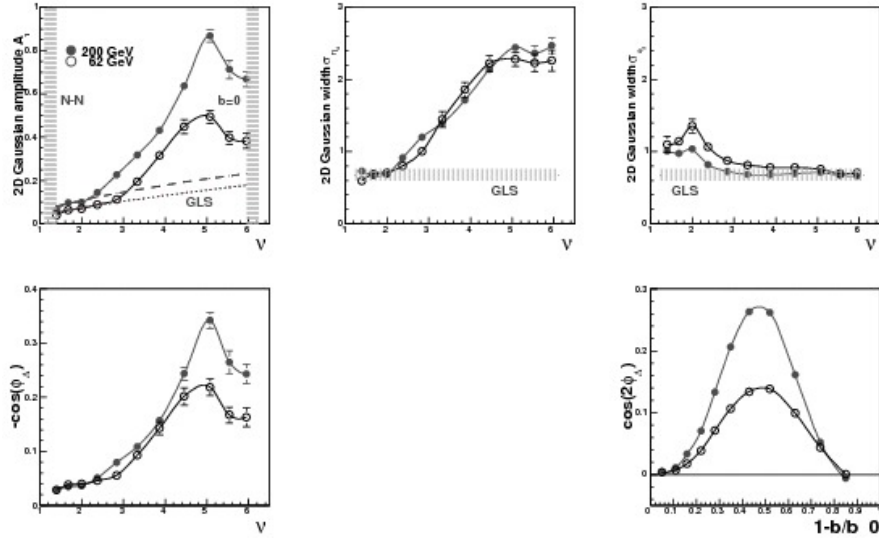


**Figure 9:** Values of fit parameters for Au-Au collision systems. For the more peripheral data the SS peak amplitude follows the binary scaling expectation, exceeding it dramatically at a transition centrality that depends on the energy/collision system. The AS ridge follows this trend very closely and the  $\eta_\Delta$  width of the SS peak also increases substantially at a similar centrality. In contrast the  $\phi_\Delta$  width of the SS peak decreases with increasing centrality and the  $\cos(2\phi_\Delta)$  term has an interesting but smooth evolution, already having a significant value before the transition centrality.

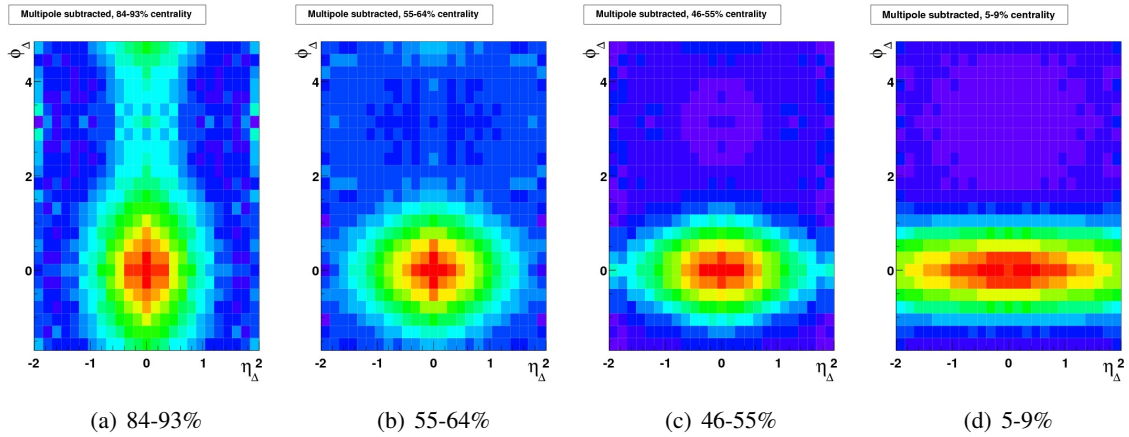


**Figure 10:** Samples of  $(\eta_\Delta, \phi_\Delta)$  correlations for 200 GeV Au-Au collisions after multipoles and sharp peak have been subtracted and plotted in a 1:1 aspect ratio. Panel 10(a) is most peripheral (84-94%) while panel 10(b) is nearly central. The middle two panels are on either side of the sharp transition, 55-64% and 46-55% centralities.

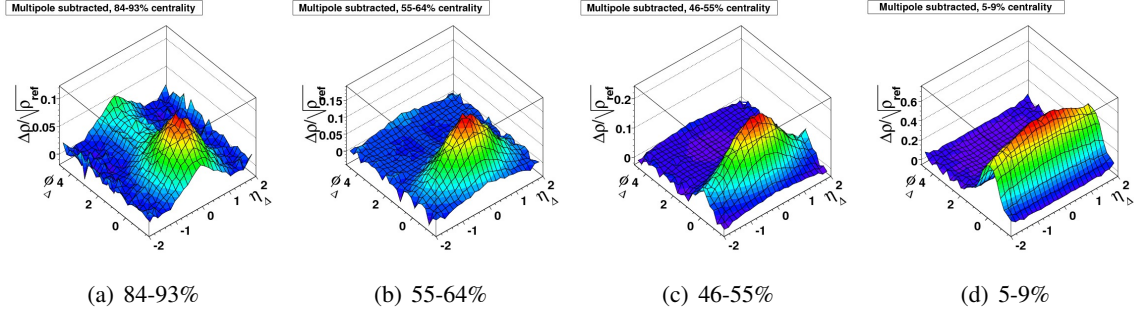


**Figure 11:** The same centralities as Fig. 10 but plotted in a view similar to Fig. 8. We have subtracted the fitted dipole, quadrupole and sharp exponential peak from the data and rotated slightly. We see the dipole and quadrupole terms have exhausted the  $\phi_\Delta$  dependent structure on the AS.

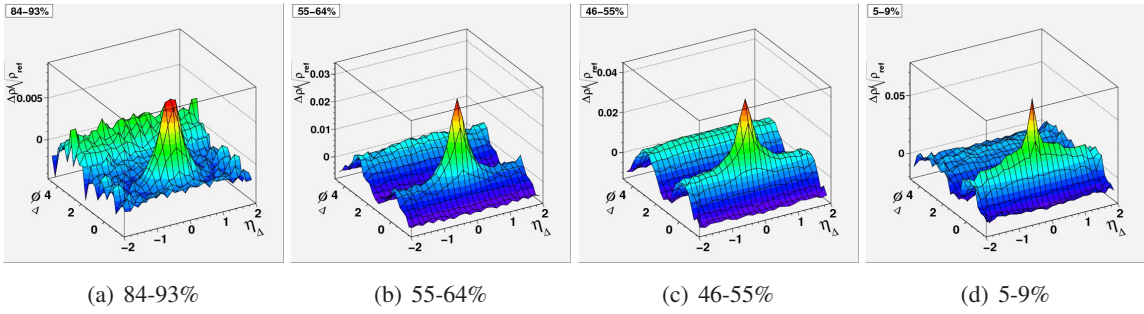


**Figure 12:** Samples of  $(\eta_\Delta, \phi_\Delta) p_t$  correlations for 200 GeV Au-Au collisions. These are the same centralities shown in Fig. 8.

We believe this peak is due to hard scattering (it certainly is for peripheral collisions) and in any case this shape cannot be due to a medium response from a pressure gradient.

## 5. $p_t$ correlations

We now return to the topic of  $p_t$  correlations which we mentioned briefly in section 1. For number correlations the Pearson's correlation coefficient quantifies how the number density at two locations vary with respect to each other. One could also ask how the total momentum densities are correlated. This turns out to be still dominated by number correlations. We instead ask how the mean  $p_t$ s are correlated. Specifically,

$$\frac{\Delta\rho}{\sqrt{\rho_{ref}}} = \frac{\overline{(p_t - n\hat{p}_t)_a(p_t - n\hat{p}_t)_b}}{\sqrt{\bar{n}_a\bar{n}_b}},$$

where  $\hat{p}_t$  is the mean  $p_t$  of the parent population. We show examples of these correlations in Fig. 12. There is a qualitative similarity with the number correlations but there are quantitative differences. Even the most peripheral bin shows no indication of a 1D Gaussian on  $\eta_\Delta$ . The sharp peak at  $(0,0)$  is dominated by HBT, opposed to number correlations where  $e^+e^-$  is a significant contribution. The broader peak centered at  $(0,0)$  is a 2D Gaussian for number correlations but has a catenary shape on  $\eta_\Delta$  for  $p_t$  correlations.

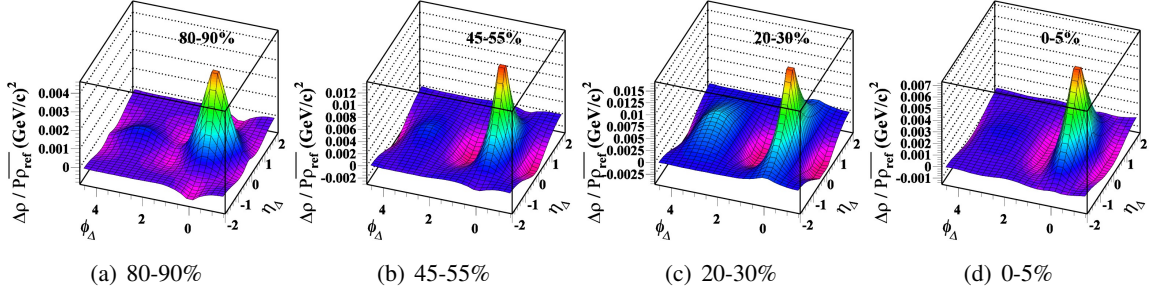


**Figure 13:**  $p_t$  correlations for 200 GeV AuAu collisions for various centralities. These correlations have been inferred from the inversion of scaled fluctuations and we have subtracted the multipoles. The shapes of the peaks at  $(0,0)$  are different than those of number correlations and there is a “recoil” hole around the peak.

We previously looked at mean- $p_t$  correlations when we were measuring  $p_t$  fluctuations and found we could invert fluctuation scale dependence to obtain detector-acceptance-independent correlations [18]. We found that the SS 2D peak amplitude was nearly proportional to the mean participant path length ( $v$ ) from the most peripheral to about 30% most-central, falling for the most central. As the centrality selection increased the SS 2D  $\eta_\Delta$  width increased by about 60% while the  $\phi_\Delta$  width decreased by about 30%. These trends are qualitatively similar to number correlations but quantitatively very different. In addition, there appears to be a “recoil hole” around the SS peak [18] which is not observed in number correlations. We also found that although Hijing does produce a SS 2D peak and an AS ridge in  $p_t$  correlations these are nearly centrality independent as well as having the wrong detailed shape, with no indication of a recoil hole [18]. We are presently working on a detailed description of these correlations to characterize our direct  $p_t$  correlation measurements.

## 6. Summary

We have presented a detailed differential analysis of minimum-bias jet systematics in p-p collisions. We have described low- $Q^2$  jets using fragmentation function systematics. The widths of the same-side (SS) 2D peak depend on the  $y_{t\Sigma}$  of the pair, changing from elongation along  $\phi_\Delta$  to symmetry in  $(\eta_\Delta, \phi_\Delta)$ , eventually reaching a width described by  $k_t$  scaling as  $y_{t\Sigma}$  is increased. We found that  $k_t$  not only affects the away-side (AS) angular correlations but also broadens the AS  $(y_{t1}, y_{t2})$  correlations.

For A-A collisions we saw that the SS 2D peak elongates along  $\eta_\Delta$ , the width increasing rapidly at a particular centrality (sharp transition). The amplitude of the SS peak is consistent with binary scaling for peripheral collisions and greatly exceeds binary-collision scaling starting near the same centrality where the  $\eta_\Delta$  width elongation starts. The AS dipole amplitude closely follows the SS 2D Gaussian peak amplitude. In contrast, the  $\phi_\Delta$  width of the SS Gaussian decreases slightly with increasing centrality. The quadrupole component is small for peripheral and central collisions but has already become significant before the transition centrality, where particle densities are low. There is no evidence for an opaque core. All partons, even low- $Q^2$  partons, are accounted for in the

final state. We are currently studying  $p_t$  correlations which provide complementary information on jets.

## References

- [1] T. A. Trainor, (2000) [hep-ph/0001148]
- [2] E. A. De Wolf, I. M. Dremin and W. Kittel, *Physics Reports* **270** (1996) 1-141
- [3] A. Bialas and R. Peschanski, *Nucl. Phys B* **273** (1986) 703-718
- [4] I. M. Dremin, O. V. Ivanov, S. A. Kalinin, K. A. Kotelnikov, V. A. Nechitailo and N. G. Polukhina, *Phys. Lett. B* **499** (2001) 97-103
- [5] T. A. Trainor, J. G. Reid, (2003) [math-ph/0304010]
- [6] T. A. Trainor, R. J. Porter and D. J. Prindle, *J. Phys. G* **31** (2005) 809 [hep-ph/0410182]
- [7] A. Bialas, (1991) *Phys. Lett. A* **525** 345-360
- [8] K. Kadija, P. Seyboth, (1992) *Phys. Lett. B* **287** 363-367
- [9] R. L. Ray, R. S. Longacre, [nucl-ex/0008009]
- [10] J. Adams et al. (STAR Collaboration), *Phys. Rev. C* **73** (2006) 64907 [nucl-ex/0411003]
- [11] S. Catani, Y. L. Dokshitzer, M. H. Seymour and B. R. Webber, *Nucl. Phys. B* **406** (1993) 187
- [12] S. D. Ellis and D. E. Soper, *Phys. Rev. D* **48** (1993) 3160
- [13] Matteo Cacciari, Gavin P. Salam, *Phys. Lett. B* **641** (2006) 57 [hep-ph/0512210]
- [14] K. Pearson *Phil. Trans. Royal Soc.* **187** (1896) 253
- [15] A. N. Tychonoff, *Doklady Akademii Nauk SSSR* **39** (1943) (5): 195-198
- [16] D. J. Prindle, T. A. Trainor, *J. Phys.: Conf. Ser.* **27** (2005) 118 [hep-ph/0506173]
- [17] J. Adams et al. (STAR Collaboration), *Phys. Rev. C* **71** (2005) 064906 [nucl-ex/0407001]
- [18] J. Adams et al. (STAR Collaboration), *J. Phys. G* **32** (2006) L37 [nucl-ex/0509030]
- [19] J. Adams et al. (STAR Collaboration), *Phys. Rev. D* **74** (2006) 032006 [nucl-ex/0606028]
- [20] S. Albino, B. A. Kniehl, and G. Kramer, *Phys. Rev. D* **73** (2006) 054020 [hep-ph/0510319]
- [21] T. A. Trainor and D. T. Kettler, *Phys. Rev. D* **74** (2006) 034012 [hep-ph/0606249]
- [22] R. P. Feynman, R. D. Field and G. C. Fox, *Nuclear Physics B* **128** (1977) 1-65
- [23] A. L. S. Angelis et al. (CCOR Collaboration), *Physics Letters B* **97** (1980) 163-168
- [24] J. Jia, *J. Phys. G* **31** (2005) S521 [hep-ex/0409024]
- [25] J. Rak, *J. Phys. G* **30** (2004) S1309 [hep-ex/0403038]
- [26] R. J. Porter and T. A. Trainor (STAR Collaboration), *Journal of Physics: Conference Series* **27** (2005) 98 [hep-ph/0506172]
- [27] M. J. Tannenbaum, *Journal of Physics: Conference Series* **27** (2005) 1 [nucl-ex/0507020]
- [28] T. A. Trainor, *Phys.Rev.C* **81**, 014905 (2010) [hep-ph/09041733]